A vented corn starch dust explosion in an 11.5 m3 vessel: Experimental and numerical study

N.B. When citing this work, cite the original published paper.

(article starts on next page)

Contents lists available at ScienceDirect

Journal of Loss Prevention in the Process Industries

A vented corn starch dust explosion in an 11.5 m³ vessel: Experimental and numerical study

Chen Huang [a,*], Marius Bloching [b], Andrei N. Lipatnikov [c]

[a] *RISE Research Institute of Sweden, Division Safety and Transport, Safety Research Department, Box 857, 501 15, Borås, Sweden*
[b] *IND EX® - Intercontinental Association of Experts for Industrial Explosion Protection e.V, Friedrich-Ebert-Anlage 36, 60325, Frankfurt am Main, Germany*
[c] *Chalmers University of Technology, Department of Mechanics and Maritime Sciences, 412 96, Gothenburg, Sweden*

ARTICLE INFO

ABSTRACT

A vented corn starch dust explosion in an 11.5 m³ vessel is studied using both experimental and numerical methods. The reduced explosion overpressure in the vessel is recorded using two pressure sensors mounted on the wall inside of the vessel. Unsteady three-dimensional Reynolds-Averaged Navier-Stokes simulations of the experiment are performed using the Flame Speed Closure (FSC) model of the influence of turbulence on premixed combustion. The model was thoroughly validated in previous studies and was earlier implemented into Open-FOAM CFD software. The self-acceleration of a large-scale flame kernel is associated with the influence of combustion-induced pressure perturbations on the flow of unburned reactants ahead of the kernel. Accordingly, the FSC model is extended by adapting the well-known experimental observations of the self-similarity of the kernel acceleration. Influence of different turbulence models on the simulated results is also explored. Thanks to the extension of the FSC model, the measured time-dependence of the pressure is well predicted when the k-omega-SST turbulence model is used.

1. Introduction

Dust explosion is a great threat to industries which deal with combustible solids, e.g., woodworking, metal processing, food and feed, pharmaceuticals and additive industries. This complicated physical and chemical process involves ignition of very fine combustible particles well mixed with air in a confined equipment, followed by a violent and explosive combustion. Once dust explosion occurs, the generated high-pressure waves, hot flames and flying fragments can cause serious loss of life and severe economic consequences. Note that a secondary explosion triggered by a primary explosion can lead to even more devastating consequences (Eckhoff, 2003).

To minimize dust explosion risks, there are various efficient methods such as training the staff to raise awareness of the explosion hazards, proper housekeeping, maintenance, procedures for hot work permit, etc. At the same time, the regulations and standards should be followed to maintain a safe working place, e.g., the use of a proper and appropriately certified equipment in explosive atmospheres to avoid ignition or installation of explosion protection systems such as venting, suppression, isolation, and containment.

The current standards handling protective systems for dust and gas

explosion venting, such as NFPA 68 (2018), EN 14491 (2012), EN 14994 (2007), and VDI 3673 (2002), are based on conservative empirical models that mostly neglect effects due to more complex geometry. This limitation reduces predictive capabilities of such models for some specific cases. For example, NFPA 68 (2018) standard was reported to yield the maximum explosion pressure for hydrogen, which was higher by a factor of 7.1 when compared to experimental data obtained in a medium-sized room (Tolias et al., 2018). Moreover, in NFPA 68 (2018) and EN 14491 (2012) standards, the geometry of an elongated enclosure is simply considered by solely using a length-to-diameter ratio, L/D. Such a simplification usually leads to a conservative estimate of explosion vent area.

The need for development of more accurate numerical tools for designing vent protection systems is motivated by the following challenges. First, the numerical model and tool can be used for conditions when the current standards are not valid or sometimes over-conservative. For example, neither NFPA 68 (2018) nor EN 14491 (2012) standard is applicable for vessels larger than 10 000 m³. Furthermore, the main equations (Eqs. (2)–(5) in EN 14491:2012) for calculating the vent area of isolated enclosures in EN 14491 (2012) require a L/D between 1 and 20. NFPA 68 (2018) gives some engineering

* Corresponding author. Box 857, 501 15, Borås, Sweden.
  E-mail address: chen.huang@ri.se (C. Huang).

guidance on venting of L/D ratios of 6 or greater, but the result is less precise than the main equations (Eqs. 8.2.1.1 and 8.2.2.3 in NFPA 68: 2018) which are limited to $L/D \leq 6$ and for some cases $L/D \leq 8$. Another example is that pre-pressurized processes are more and more required to be protected by the industry, especially in the chemical industry such as reactors. However, elevated pressures are not yet considered in the EN 14491 (2012) or in the EN 14994 (2007) standard. One more example is gas or dust explosion in complex geometries, where the current standards are not applicable or yield very conservative and, therefore, uneconomical vent areas. Furthermore, there is a need for optimization of vent areas in large vessels, where it can be expected that homogenous dust distribution is unlikely. Accordingly, explosion overpressures are lower, which implies that smaller vent areas would be acceptable.

It is worth noting that, due to the lack of required data, a dust explosion is a much more challenging process for Computational Fluid Dynamics (CFD) modelling when compared to a gas explosion. Indeed, even for the most studied dust, corn starch, information about particle size distribution, particle agglomeration (Eckhoff, 2020), and fundamental dust flame characteristics, e.g., the laminar flame speed (Phylaktou et al., 2010), is limited. Nevertheless, in spite of these limitations, CFD simulations of dust explosions were performed by various research groups adopting different methods and numerical tools.

Typically, dust explosion CFD simulations are performed using a commercial code FLACS-DustEx, which was initially developed within a European Union project in 2002–2005. The code is based on assumptions that (i) a dust flame resembles that of a gas flame for fine dust with high volatile content, and (ii) there is thermal and kinetic equilibrium between dispersed particles and continuous phase (Skjold, 2014a). Results of such dust explosion simulations were compared with experimental data measured in (i) a 9.4 m³ silo (Skjold et al., 2005), (ii) interconnected vessels with volumes of 2, 4 and 20 m³ (Skjold et al., 2005; Skjold, 2007), and (iii) a 236 m³ silo (Skjold et al., 2006). The focus of those studies was placed on the maximum reduced explosion overpressures, whereas major transient characteristics of flame kernel expansion (e.g., the flame propagation speed or the explosion overpressure trace) were not addressed in the cited papers. As discussed in detail elsewhere (Skjold 2014b), there is still space for improving the FLACS-DustEx code in various ways, e.g., (i) adoption of an unstructured grid to resolve curved surfaces, (ii) a wider choice of turbulence models in addition to the standard k-epsilon model (Launder and Spalding, 1972), (iii) an improved combustion model with reduced grid resolution dependency, etc.

Besides the FLACS-DustEx code, general-purpose commercial CFD codes were also applied for simulating dust explosions. For example, corn starch dust explosion in a standardized test 20 l vessel was recently simulated using Lagrangian particle tracking and the Eddy Break-Up (EBU) combustion model (Li et al., 2020). Moreover, a hybrid mixture explosion in a 20 l vessel was simulated using a similar approach but another CFD code (Pico et al., 2020). Note that the EBU combustion model was originally developed for gaseous flames (Spalding, 1971; Magnussen and Hjertager, 1977) and it has been implemented into almost all commercial CFD codes aiming at computations of gaseous flames. Thus, similarly to the aforementioned studies that adopted the FLACS-DustEx code, the recent studies by Li et al. (2020) and Pico et al. (2020) were also based on an analogy between dust explosions and premixed turbulent flames.

The present paper reports results obtained within the framework of an ongoing research project aiming at development of advanced models and numerical tools for simulating dust explosions in the process industries. The developed approach is based on the same analogy between dust explosions and premixed turbulent flames. Accordingly, to simulate dust explosion, a model of the influence of turbulence on premixed combustion is adapted in the present work. More specifically, the socalled Flame Speed Closure (FSC) model (Lipatnikov and Chomiak, 1997, 2002) is used. In the preceding study (Huang et al., 2020), (i) the FSC model was implemented into the OpenFOAM code, (ii) the
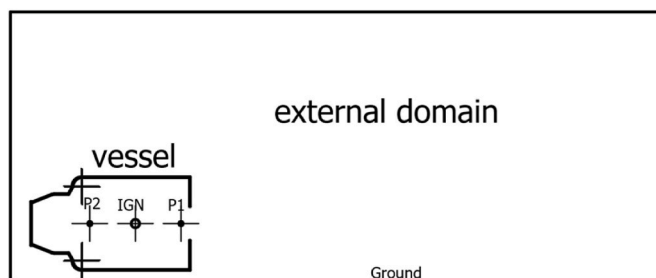

Fig. 1. 2-Dimensional drawing of the 11.5 m³ explosion vessel and the computational domain.

Fig. 2. Vented corn starch dust explosion in the 11.5 m³ vessel.

implementation was verified using benchmark analytical solutions, and (iii) the FSC model and the so-extended code were validated against experimental data on corn starch dust explosions obtained in a small-scale fan-stirred vessel (Bradley et al., 1989). The present paper reports new results obtained by applying the model and code and extending them in order to run unsteady three-dimensional Reynolds-Averaged Navier-Stokes (RANS) simulations of an experimentally investigated industrial relevant vented explosion.

In the next section, the experiment setup, method, and results are briefly summarized. Numerical method and setup are described in Section 3. Computed results are presented and discussed in Section 4, followed by conclusions.

2. Experimental method and setup

An 11.5 m³ vessel at the REMBE® Research + Technology Center in Brilon, Germany was used to perform vented corn starch dust explosions. The corn starch used was a St1 dust having a K_{St}-value of 200 bar m/s ± 15%. The calculated and applied vent area was set to 0.5 m² in a circular shape, equalling an 800 mm diameter vent opening. The vent opening was closed with a layer of 70 μm low mass aluminium foil, which showed to have a static activation pressure (p_{stat}) of 0.1 ± 15%.

To create an explosive atmosphere inside the vessel two pressured dust containers were used for blowing the dust into the test vessel. A concentration of 750 g/m³ was selected. An ignition delay of 800 ms was set via multiple tests in order to achieve the required K_{St}-value with the above dust concentration.

The resulting explosive atmosphere was ignited using pyrotechnique igniters with an ignition energy of 2 × 5 kJ in the center of the test vessel. For detection of the reduced maximum explosion

Table 1
Summary of thermophysical properties of corn starch dust.

Description	Symbol	value
Chemical formular	$C_6H_{7.88}O_{4.98}$	
Molecular weight	W_{cs}	0.16 kg/mol
Standard heat of formation	$H_{f,cs}^{\ominus}$	−792.6 kJ/mol
JANAF coefficients	$a_{0,cs}$	− 3.2726
	$a_{1,cs}$	0.10056
	$a_{2,cs}$	0
	$a_{3,cs}$	0
	$a_{4,cs}$	0
	$a_{5,cs}$	−9 9808

overpressures (p_{red}) inside the vessel, two pressure detectors P1 and P2 were installed (see Fig. 1). The data was recorded using an oscilloscope (Tektronix TDS, 2014C). A snapshot of the vented corn starch dust explosion is shown in Fig. 2.

3. Numerical method and setup

3.1. Thermophysical properties of corn starch dust

Thermophysical properties of dust are required for calculating the mass and heat transfer processes in a CFD simulation. These properties involve the dust chemical formula (e.g., the molecular weight is calculated using the formula), heat of reaction, standard heat of formation, specific heat capacity, and adiabatic flame temperature.

In this work, the chemical formula of $C_6H_{7.88}O_{4.98}$ is used for corn starch following Bradley et al. (1989). Based on this formula, a molecular weight of corn starch W_{cs} is set equal to 0.16 kg/mol. The standard heat of formation of corn starch is set equal to $H_{f,cs}^{\ominus}$ = -792.6 kJ/mol or −4970 kJ/kg. The latter value is obtained by assuming the complete combustion of corn starch and using the value of $\Delta H_{reaction}$ = 2521 kJ/mol for the heat of reaction, reported by Bradley et al. (1989).

The specific heat capacity of corn starch was measured by Tan et al. (2004) and was fitted using a linear function with temperature. Within the framework of the OpenFOAM platform, the NIST-JANAF polynomial equations are used to calculate the specific heat capacity c_p [J/(kg K)] and the so-called absolute enthalpy H_a [J/kg] as follows

$$c_{p,cs} = R_{spec,cs}\left(a_{4,cs}T^4 + a_{3,cs}T^3 + a_{2,cs}T^2 + a_{1,cs}T + a_{0,cs}\right) \quad (1)$$

$$H_{a,cs} = R_{spec,cs}\left(\frac{a_{4,cs}}{5}T^5 + \frac{a_{3,cs}}{4}T^4 + \frac{a_{2,cs}}{3}T^3 + \frac{a_{1,cs}}{2}T^2 + a_{0,cs}T + a_{5,cs}\right) \quad (2)$$

Here, $R_{spec,cs} = R_0/W_{cs} = 52.11$ is the specific gas constant for corn starch measured in J/(kg·K); $R_0 = 8.314$ J/(mol·K) is the ideal gas constant; $a_{0,cs}, a_{1,cs}, a_{2,cs}, a_{3,cs}, a_{4,cs}$ and $a_{5,cs}$ are the JANAF coefficients. A summary of all the thermophysical properties of corn starch dust is shown in Table 1.

3.2. Laminar burning velocity of corn starch dust

Contrary to gaseous flames, available data on the laminar burning velocity are very limited and controversial for dust corn starch. Measurements of this velocity are difficult for a number of reasons. First, when applied to dust-air mixtures, high-speed schlieren photography, which is the standard technique for measuring speeds of gaseous laminar flames, has unfavourable optical properties (Dahoe and de Goey, 2003). Second, there is a difficulty in balancing between dust settlement and a laminar flow in experiments (Proust, 1993; Van Wingerden et al., 1996; Phylaktou et al., 2010). Third, certain dust properties, e.g., particle size or moisture content, substantially affect the laminar burning velocity of a dust-air cloud but are rarely reported in the experimental papers.

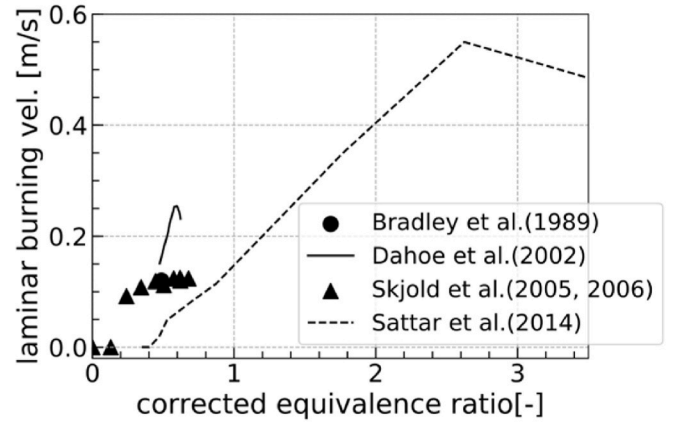For these and other reasons, the published data on the laminar

Fig. 3. Comparison of laminar burning velocities for corn starch dust reported by Bradley et al. (1989), Dahoe et al. (2002), Skjold et al. (2005, 2006), and Sattar et al. (2014).

burning velocities of mixtures of corn starch dust with air poorly match each other, see Fig. 3. Note that the data by Bradley et al. (1989) and by Dahoe et al. (2002) were originally reported vs. dust concentration. In Fig. 3, the dust concentration is converted to a corrected equivalence ratio using data on burnt mass fraction reported in papers by Skjold et al. (2005, 2006). The corrected equivalence ratio includes only dust which participated in the explosion.

In the present study, the laminar burning velocity measured by Dahoe et al. (2002) is used since their data resides in a medium range among the available data. The laminar burning velocity of corn starch dust measured by Dahoe et al. (2002) is approximated using the Gülder's correlation (Gülder, 1984) as follows

$$S_L = W\varphi^{\eta}e^{-\xi(\varphi-\sigma)^2}, \quad (3)$$

Here, the coefficients $W = 0.2145$, $\eta = -0.2774$, $\xi = 39.1832$, $\sigma = 0.6$ for corn starch dust. Note, that the method used to set initial conditions in the present simulations offers an opportunity to mitigate the influence of eventual errors in the adopted values of the laminar burning velocity on the computed results, as discussed in Sect. 4.

3.3. Turbulence models

OpenFOAM offers a substantial number of turbulence models. In this paper, the following turbulence models for unsteady and compressible RANS simulations are used:

(i) the standard k-epsilon (Launder and Spalding, 1972, 1983; El Tahry, 1983),
(ii) realizable k-epsilon (Shih et al., 1994, 1995),
(iii) RNG k-epsilon (El Tahry, 1983; Yakhot et al., 1992),
(iv) Launder-Sharma k-epsilon (Launder and Sharma, 1974; El Tahry, 1983),
(v) k-omega (Wilcox, 1998),
(vi) k-omega-SST (Hellsten, 1998; Menter and Esch, 2001; Menter et al., 2003),
(vii) SSG (Daly and Harlow, 1970; Speziale et al., 1991).

Note that for all these models the default coefficients provided in OpenFOAM are used with the exception of the turbulent Prandtl number which is set equal to 0.28 following our previous study (Huang et al., 2020).

Moreover, a test simulation was also performed to account for the dilatation effect due to heat release during the burning process following the work by Chomiak and Nisbet (1995). Specifically, the coefficient C_3 used in the epsilon equation was changed from 0 (default value) to

−0.33 (dilatation effect). The simulation results show that this change in coefficient slightly increases the calculated explosion overpressure but does not contribute significantly to the pressure rise rate.

3.4. FSC combustion model

Since both the FSC model of the influence of turbulence on premixed combustion and validation of this model are discussed in detail in a monograph by Lipatnikov (2012), review papers (Lipatnikov and Chomiak, 2002; Lipatnikov, 2018) and in the preceding paper by the present authors (Huang et al., 2020), we will restrict ourselves to listing the key model equations.

The FSC model deals with the following transport equation

$$\frac{\partial \overline{\rho}\, \widetilde{c}}{\partial t} + \nabla \cdot (\overline{\rho}\, \widetilde{\mathbf{u}}\, \widetilde{c}) = \nabla \cdot [\overline{\rho}(\kappa + D_t)\nabla \widetilde{c}] + \rho_u U_t |\nabla \widetilde{c}| + \frac{\overline{\rho}(1-\widetilde{c})}{t_r(1+D_t/\kappa_b)}\exp\left(-\frac{\Theta}{\widetilde{T}}\right),$$
(4)

for the Favre-averaged combustion progress variable $\widetilde{c}$. Here, t is the time; $\mathbf{u}$ is the flow velocity vector; κ is the molecular heat diffusivity of the mixture; the Favre-averaged temperature $\widetilde{T}$ is evaluated using the simplest form $\overline{\rho}\widetilde{T} = \rho_u T_u$ of the ideal gas state equation; Θ is the activation temperature for a single reaction that the combustion chemistry is reduced to ($\Theta = 20000$ K in the present work); over-lines designate the Reynolds average, while $\widetilde{q} = \overline{\rho q}/\overline{\rho}$ is the Favre-averaged value of q with $q'' = q - \widetilde{q}$; subscripts u and b designate unburned and burned gas, respectively.

The reaction time scale t_r in the last source term on the right-hand-side of Eq. (3) is set so that, at the limit of vanishing rms turbulent velocity, i.e., $u' \to 0$, the burning velocity yielded by the model in the stationary one-dimensional case is equal to the laminar burning velocity S_L, which is an input parameter of the model. This constraint results in

$$t_r = \Psi^2\left(\frac{T_b}{T_u}, \frac{\Theta}{T_u}\right) \frac{\kappa_u}{S_L^2},$$
(5)

where the non-dimensional function Ψ approximates values of $S_L\sqrt{t_r/\kappa_u}$. A polynomial fit to the function Ψ, which features no tuning parameter and was reported by Huang et al. (2016), is used here.

The mean density is given by the following well-known Bray-Moss-Libby (BML) equations (Bray and Moss, 1977; Libby and Bray, 1977)

$$\overline{\rho} = \frac{\rho_u}{1 + (\sigma - 1)\widetilde{c}}, \quad \overline{\rho c} = \rho_b \overline{c};$$
(6)

where $\sigma = \rho_u/\rho_b$ is the density ratio.

The turbulent diffusivity D_t and burning velocity U_t are closed as follows (Lipatnikov and Chomiak, 1997)

$$D_t = D_{t,\infty}\left[1 - \exp\left(-\frac{t_{fd}}{\tau_L}\right)\right],$$
(7)

$$U_t = U_{t,ISP}\left[1 - \frac{\tau_L}{t_{fd}} + \frac{\tau_L}{t_{fd}}\exp\left(-\frac{t_{fd}}{\tau_L}\right)\right]^{1/2},$$
(8)

where t_{fd} is the flame development time counted starting from ignition; $D_{t,\infty}$ is the fully developed turbulent diffusivity given by a turbulence model; $\tau_L = D_{t,\infty}/u'^2$ is the Lagrangian time scale of turbulence;

$$U_{t,ISP} = Au' Da^{1/4}$$
(9)

is an intermediately steady turbulent burning velocity (Zimont, 2000); $Da = \tau_t/\tau_f$ is the Damköhler number; $\tau_t = L/u'$ and L are turbulent time and length scales, respectively; $\tau_f = \delta_L/S_L$ and $\delta_L = \kappa_u/S_L$ are the laminar flame time scale and thickness, respectively; $A = 0.4$ is the sole constant of the FSC model.

The reader interested in a more detailed discussion of the FSC model

and its validation is referred to the aforementioned monograph by Lipatnikov (2012) and review papers (Lipatnikov and Chomiak, 2002; Lipatnikov, 2018).

3.5. An extension of the FSC model

The FSC model addresses the influence of turbulence on combustion but does not allow for the influence of combustion-induced thermal expansion on turbulence. The latter influence should be addressed by a turbulence model. However, in spite of long-term research into such thermal expansion effects and a number of important phenomena found in experimental and direct numerical simulation studies reviewed elsewhere (Lipatnikov and Chomiak, 2010; Sabelnikov and Lipatnikov, 2017) a model with well-documented capabilities for predicting effects of thermal expansion on turbulence in premixed flames has not yet been developed. Nevertheless, such effects should be considered in a CFD study of a gaseous or dust explosion, because they cause significant self-acceleration of a growing flame kernel (Bauwens et al., 2008, 2011, 2015). In such a challenging situation, a simple semi-empirical approach is chosen in the present work as a solution for applied CFD research into large-scale explosions.

The approach is based on a seminal study by Gostintsev et al. (1988) who analysed a large amount of experimental data obtained in large-scale experiments with growing flame kernels. Their analysis revealed a self-similar regime of flame kernel growth, characterized by the following empirical relation for the flame kernel radius

$$R_f(t) = R_{f,0}\left(\frac{t}{t_0}\right)^{3/2}.$$
(10)

While the "initial" (for this regime, but not for the flame kernel ignition) values of the flame radius $R_{f,0}$ and time t_0 depend on mixture composition and other experimental conditions, the same power exponent 3/2 fits well to all data analysed by Gostintsev et al. (1988). Subsequently, the existence of such a regime was supported in an experimental study by Bradley et al. (2001). This regime was also addressed in other phenomenological and theoretical studies (Bradley, 1999; Gostintsev et al., 1999) but discussion of such studies is beyond the scope of the present work.

Here, based on the experimental findings briefly reviewed above, the FSC Eq. (7) is simply modified as follows

$$U_t = U_{t,ISP}\underbrace{\left[1 - \frac{\tau_L}{t_{fd}} + \frac{\tau_L}{t_{fd}}\exp\left(-\frac{t_{fd}}{\tau_L}\right)^{1/2}\right]}_{T_1}\underbrace{\left(\frac{t}{t_{flacc}}\right)^{1/2}}_{T_2},$$
(11)

where t_{flacc} is the timing for activating the flame acceleration mechanism in simulations (if $t < t_{flacc}$, the original FSC Eq. (7) is used). Due to the lack of a model or empirical formula, which could be adopted to calculate the values of $R_{f,0}$ and t_0, associated with the onset of the discussed self-similar regime, Eq. (10) requires tuning t_{flacc}. In this work, $t_{flacc} = 0.15$ s, which corresponds to a flame position characterized by $\overline{c} = 0.5$ at a distance of 1.85 m away from the vent opening.

While Eq. (10) involves two unsteady terms T_1 and T_2, these terms are associated with different physical mechanisms and control an increase in $U_t(t)$ during different time intervals. More specifically, term T_1 was theoretically obtained by Lipatnikov and Chomiak (1997) by combining a model of intermediately steady turbulent flame propagation (Zimont, 1979) with the classical theory of turbulent diffusion (Taylor, 1921, 1935; Hinze, 1975). As turbulence is mainly rotational motion, term T_1 models an increase in turbulent burning rate due to the influence of the rotational motion on a premixed flame. Moreover, this term rapidly grows from zero with time and reaches unity at $t_{fd} \gg \tau_L$. In particular, this term varies weakly and is close to unity at $t > t_{flacc}$, but plays an important role during an earlier stage of flame kernel growth. Note that during this earlier stage, the kernel self-accelerates also due to
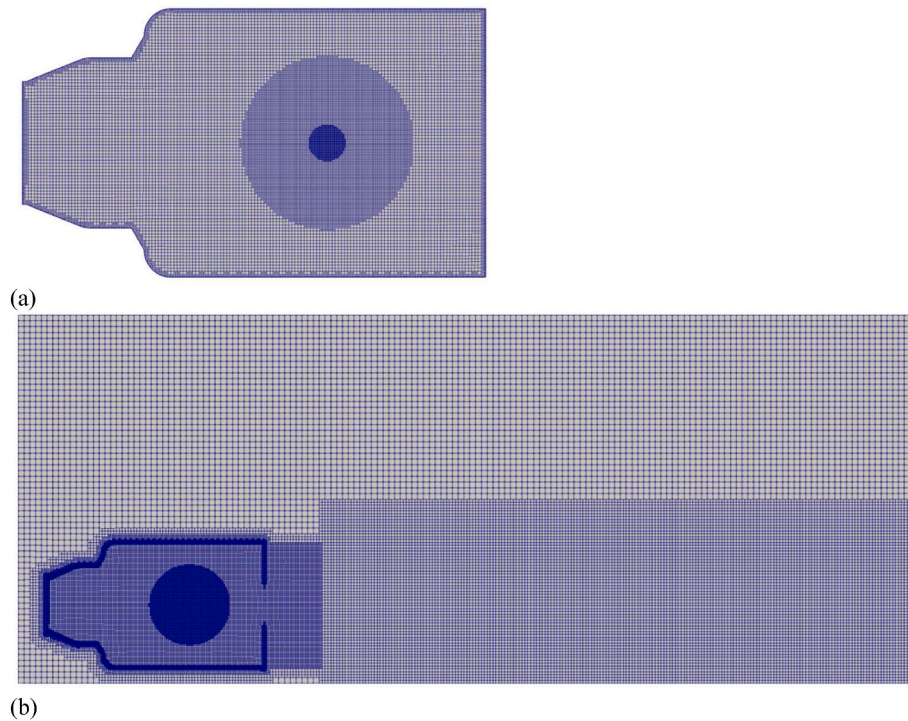
Fig. 4. Two sets of computational meshes. (a) Mesh for closed vessel. (b) Mesh for the vessel and outside domain.

a decrease in a ratio of the mean flame brush thickness to the mean kernel radius with time, as discussed in detail by Lipatnikov and Chomiak (2004, 2007). Contrary to term T_1, term T_2 plays a role only at $t > t_{flacc}$, grows from unity at $t > t_{flacc}$ to 1.4 at $t = 0.3$ms, when the overpressure peaks, and models the kernel acceleration under the influence of potential velocity fluctuations caused by rapid propagation of combustion-induced pressure perturbations into unburned mixture. Thus, terms T_1 and T_2 are associated with different types of velocity fluctuations (rotational and potential, respectively) and substantially affect the kernel growth rate during different time intervals.

3.6. Numerical setup

The vented corn starch dust explosion was simulated in two stages. First, the dust explosion was simulated in a closed vessel. When the computed overpressure in the vessel reached a critical value of 0.1 bar (recall that, in the experiments, the vent panel ruptured at a static activation pressure p_{stat} equal to 0.1 bar $\pm15\%$), the simulation was stopped, and the results were saved. These computed results were then mapped to a new computational mesh created for a larger computational domain to simulate the venting process. The large domain that was not addressed in the first-stage simulation was initialized using the temperature, pressure, and turbulence characteristics that were set as the initial conditions for the first-stage simulation. Note that the initial turbulence characteristics outside of the vessel has little influence on the burning process since most of the turbulent kinetic energy is generated during the venting process.

The CAD geometry of the vessel was constructed using an open-source 3D CAD modelling tool FreeCAD. The geometry was then imported into the OpenFOAM, and the computational mesh was generated using the so-called snappyHexMesh tool available in OpenFOAM. Accordingly, two sets of computational meshes were used for the simulations (see Fig. 4). The first mesh was used for simulating dust explosion before the rupture of the vent panel, whereas the second mesh covered the volume of the vessel and a volume outside of the vessel to capture the venting process. The first mesh (see Fig. 4a) is characterized by a mesh number of 1 348 354 and a mesh size between 6.25 and 25

Table 2
Initial conditions.

Parameters	Value
T_0 [K]	273
P_0 [Pa]	101 325
$\tilde{k}$ [m^2/s^2]	0.8438
u' [m/s]	0.75
L [m]	0.1
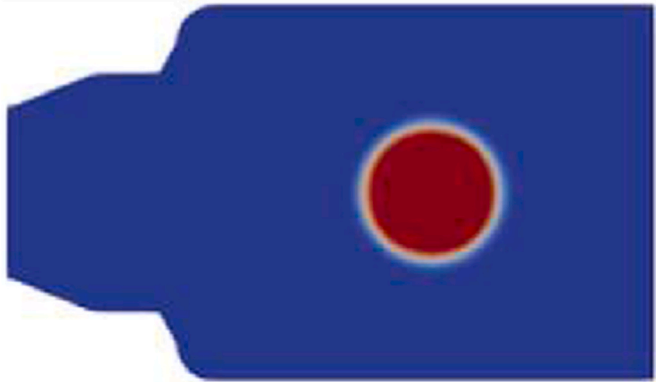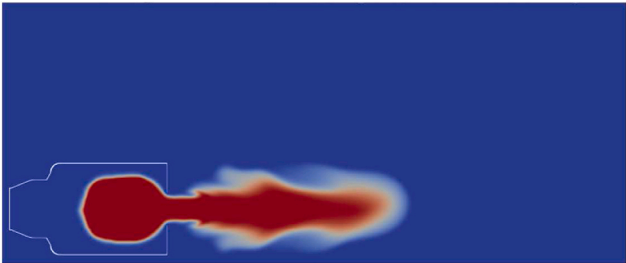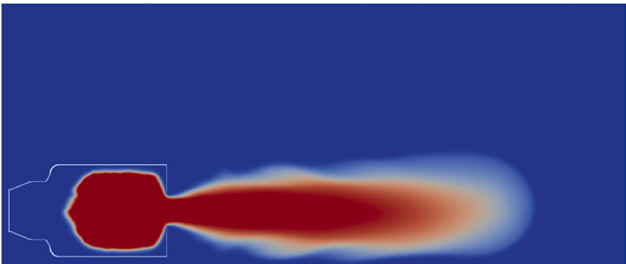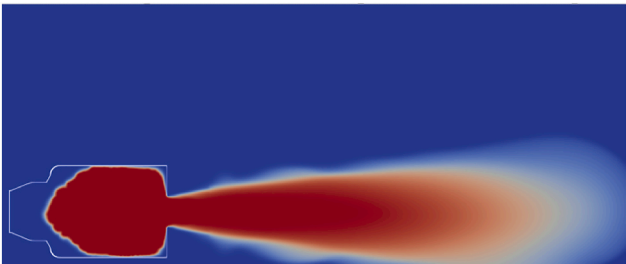
Table 3
Boundary conditions in OpenFOAM.

	walls	Open boundaries
P [Pa]	zeroGradient	totalPressure
$\tilde{\mathbf{u}}$ [m/s]	noSlip	pressureInletOutletVelocity
$\tilde{T}_u$ [K]	fixedValue 273	fixedValue 273
$\tilde{b}$ [-]	zeroGradient	zeroGradient
$\tilde{k}$ [m2/s2]	kqRWallFunction	zeroGradient

mm. It took less than 1 h to simulate the flame kernel growth until the rupture of the vent panel (duration of this physical process was about 0.1 s in the experiments and simulations) using 1 node with 28 cores. The second mesh (see Fig. 4b) covers a computational domain of 15.5 × 5 × 6.355 m. The mesh has 2 431 262 cells, with the mesh size varying between 12.5 and 100 mm. Simulations of the venting process, whose physical duration was about 0.35 s in the experiments and computations, took around three days using 2 nodes with 56 cores. Note that only a half of the computational domain was simulated to save computational time by taking advantage of symmetry on a vertical plane with respect to the ground cutting through the center of the vessel and along the length of the vessel.

The initial and boundary conditions are reported in Tables 2 and 3, respectively. The composition of the dust-air mixture was assumed to be

Table 4
Mean combustion progress variable fields computed at different time instants.

Time [s]	Reynolds-Averaged progress variable [-]
0.1	
0.15	
0.2	
0.25	
0.3	
0.35	

Table 4 (*continued*)

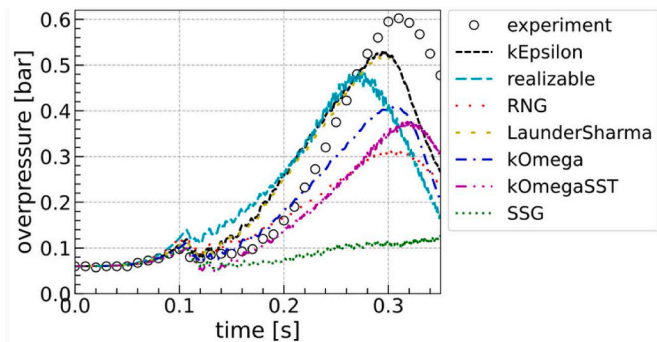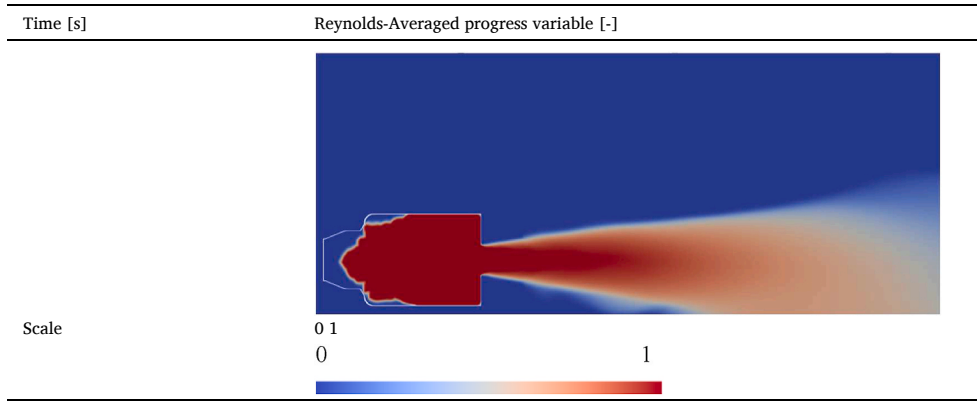| Time [s]	Reynolds-Averaged progress variable [-]
Scale	0 1

Fig. 5. Effect of different turbulence models on the calculated explosion overpressure in a closed vessel. $u' = 0.75$ m/s, $L = 0.1$ m.

spatially uniform in the closed vessel, with a dust concentration being equal to 750 g/m^3 and the corrected equivalence ratio Φ being equal to 0.62. Since the turbulence characteristics were not measured, they were guessed and, then, adjusted in order to get agreement between the overpressures $\Delta P(t)$ measured and computed under conditions of $\Delta P(t) < 0.1$ bar, i.e. when the entire flame kernel was inside the closed vessel. This method also offers an opportunity to handle uncertainties of the data on laminar burning velocities, because the computed turbulent burning velocity is affected by the Damköhler number, i.e., by a combination of the laminar flame and turbulence characteristics. Since the FSC model was already validated in a recent study (Huang et al., 2020) of dust explosion experiments performed in a small-scale vessel (Bradley et al., 1989), the focus of the present validation study was placed on assessment of the model capabilities for predicting the overpressure dynamics during the venting process.

4. Results and discussions

Table 4 shows evolution of the computed fields of the Reynolds-averaged combustion progress variable at different time instants.

Turbulence is well known to substantially affect burning process. Evolutions of corn starch dust explosion overpressures computed using the conventional FSC model, i.e., Eqs. (7) and (8), and different turbulence models are reported in lines in Fig. 5, with black circles showing the experimental data. By investigating these experimental data, four different stages could be found: (i) an increase in the overpressure during dust explosion in the closed vessel before the rupture of the vent panel, i.e., at $t < 0.1$ s, (ii) a decrease in the overpressure after the rupture of the vent panel, i.e., at $0.1 < t < 0.12$ s, followed by a slow increase in the overpressure at $0.12 < t < 0.16$ s, (iii) a rapid increase in the overpressure at $0.16 < t < 0.30$ s, and (iv) a decrease in the over-pressure at $t > 0.31$ s. Results measured or computed during stages (i)

and (ii) are zoomed in Fig. 6a and b, respectively. During stage (i), all explosion products are confined to the closed vessel. During stage (ii), the products appear outside the vessel. During stage (iii), the explosion kernel grows outside the vessel.

Fig. 5 show that realizable (cyan long-dashed lines), k-epsilon (black dashed lines), and Launder-Sharma (yellow short-dashed lines) turbulence models belong to a group which yields a fast pressure rise rate during stages (i)-(iii) of the dust explosion and the highest explosion overpressures. On the contrary, SSG turbulence model yields the slowest rate of pressure rise (green dotted lines) and the lowest explosion overpressure. During stage (ii), pressure drop computed using SSG model is significantly overestimated, with subsequent computed pressure increase being too slow. During stage (i) disagreement between the measured data and the results computed using k-epsilon, realizable, Launder-Sharma, or SSG turbulence model can be handled by adjusting the initial turbulence characteristics, which significantly affect simulated pressure curves (see Figs. 7 and 8). However, during stage (ii), such a disagreement is much more difficult to handle.

From this perspective, results obtained using RNG (red dotted lines), k-omega (blue dotted-dashed lines), and k-omega-SST (violet double-dotted-dashed lines) turbulence models appear to most promising during stage (ii), as shown in Fig. 6b. However, RNG turbulence model yields too fast pressure rise rate before the rupture of the vent panel (see Fig. 6a). If the first stage ($t < 0.1$ s) and the second stage ($0.1 < t < 0.16$ s) of the dust explosion are considered jointly, k-omega and k-omega-SST turbulence models belong to a group which yields a reasonable agreement with the experimental data. Accordingly, these two turbulence models are selected for further study, with this choice being mainly based on quite moderate rate of pressure rise, yielded by these two models at $0.1 < t < 0.2$ s (see blue and volet dotted-dashed lines in Fig. 6b).

However, Fig. 9 shows that results computed using the conventional FSC model and k-omega or k-omega-SST turbulence model substantially underestimate the measured overpressure. Fig. 11 indicates that this problem can be handled by adopting the extended FSC model, i.e., by substituting Eq. (7) with Eq. (10), which allows for the self-similar flame acceleration discovered by Gostintsev et al. (1988). Such a method requires tuning of a single input parameter, i.e., time t_{flacc} when the acceleration term is acivated in Eq. (10). Recall that Eq. (7) is used at $t < t_{flacc}$. Since the self-similar regime of flame acceleration was documented for large unconfined flames but the entire explosion kernel is sufficiently small and confined before the rupture of the vent panel at $t = 0.1$ s, the activation time t_{flacc} should definitely be well larger than 0.1 s. The use of a too small t_{flacc} results in overestimated overpressure, see cyan dashed line in Fig. 9.

Finally, comparison of red dashed lines with circles in Figs. 10 and 11 shows that the use of the extended FSC model with $t_{flacc} = 0.15$ s and standard k-omega-SST turbulence model has allowed us to well predict the measured overpressure history during all four studied stages of the
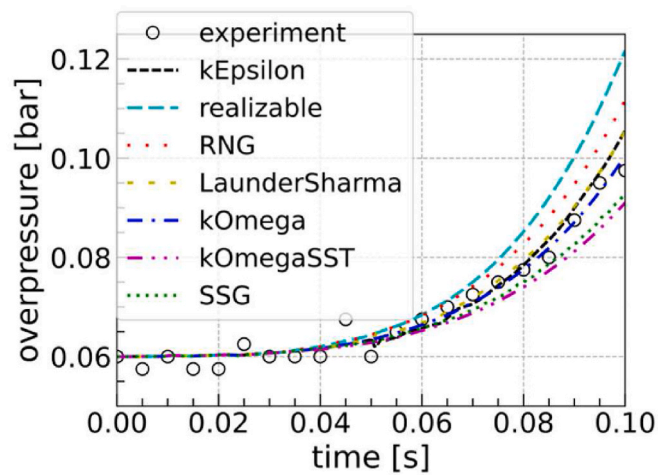
(a)
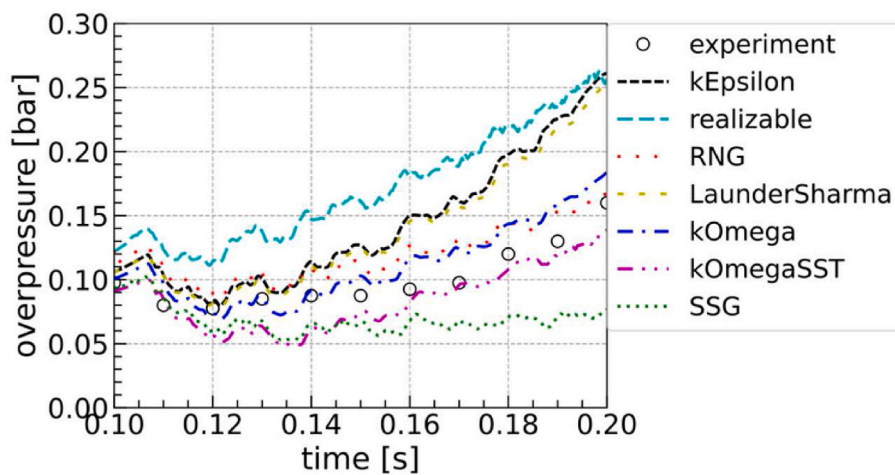
(b)

Fig. 6. Effect of different turbulence models on the explosion overpressure computed during (a) the first and (b) second stages of the dust explosion.
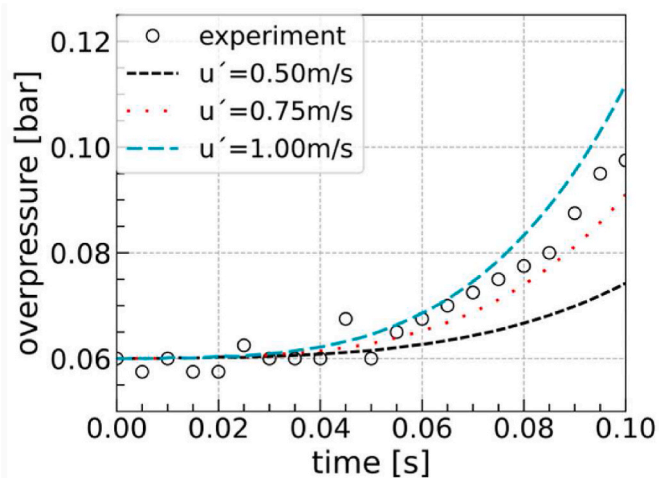

Fig. 7. Effect of turbulence velocity fluctuations u' on the calculated explosion overpressure before the rupture of the vent panel. $L = 0.1$ m, k-omega-SST turbulence model.
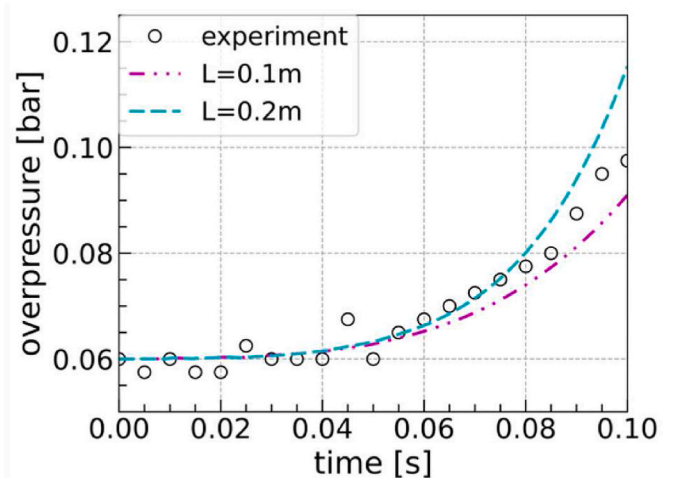

Fig. 8. Effect of turbulence length scale on the calculated explosion overpressure before the rupture of the vent panel. $u' = 0.75$ m/s, k-omega-SST turbulence model.
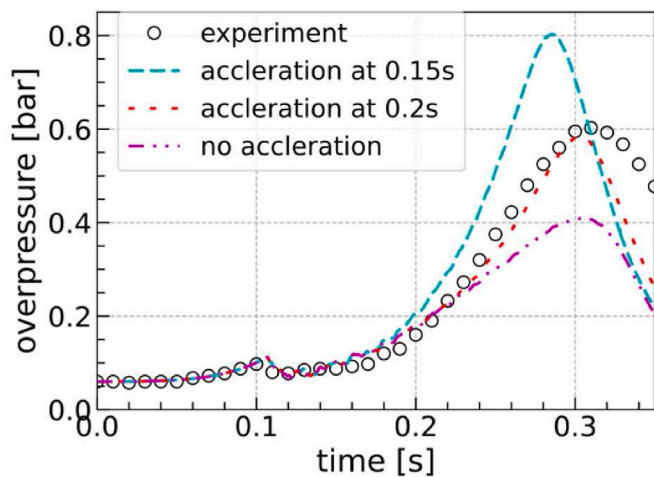
Fig. 9. Effect of flame acceleration sub-model on the calculated explosion overpressure. $u' = 0.75$ m/s, $L = 0.1$ m, k-omega turbulence model.
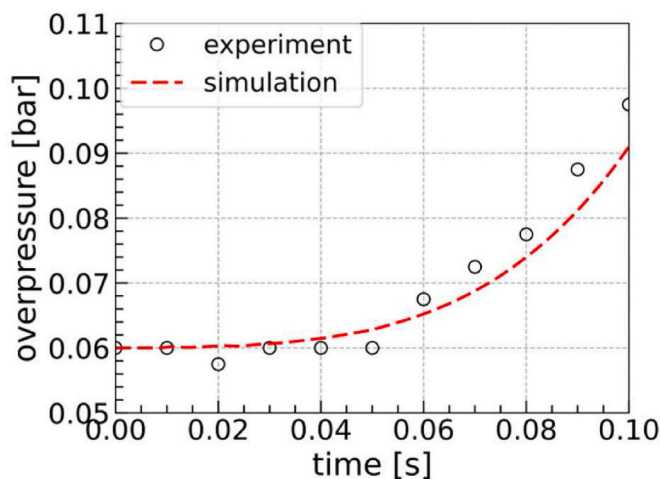

Fig. 10. Comparison between measured and simulated explosion overpressures until the rupture of the vent panel. $u' = 0.75$ m/s, $L = 0.1$ m, k-omega-SST turbulence model.
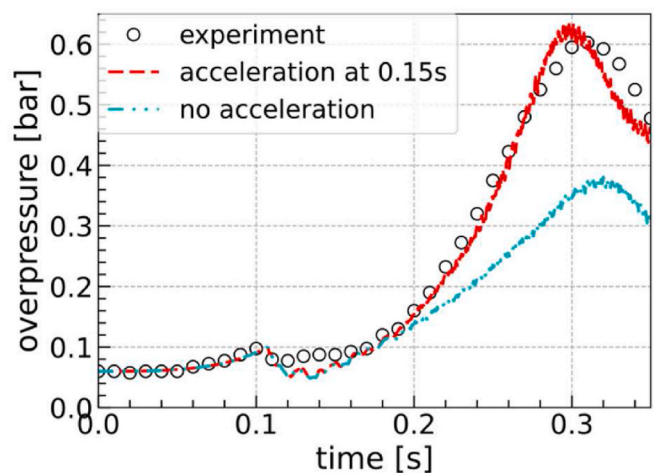

Fig. 11. Comparison between measured and simulated explosion over-pressures. $u' = 0.75$ m/s, $L = 0.1$ m, k-omega-SST turbulence model.

dust explosion. In particular, the peak overpressure and the corresponding instants are well predicted. The use of the conventional FSC model without the acceleration factor in Eq. (10) yields significantly underpredicted overpressure when compared to the experimental data, cf. cyan line with symbols in Fig. 11.

5. Concluding remarks

Vented corn starch dust explosion in an 11.5 m³ vessel was investigated experimentally and numerically. The numerical approach is based on unsteady three-dimensional RANS simulations using the FSC model of the influence of turbulence on combustion and various turbulence models implemented into OpenFOAM. Comparison of measured and computed overpressures indicates that k-omega and k-omega-SST models perform better than other explored turbulence models. While the use of the conventional FSC model yields underpredicted overpressure when compared to the experimental data, an excellent agreement between measurements and simulations was obtained by phenomenologically extending the FSC model to allow for the well-known self-similar regime of acceleration of large flame kernels, see Eq. (10). Therefore, this simple and numerically efficient extension of the FSC model looks promising and deserves further study in simulations of other large-scales dust or gaseous explosions.

Credit author statement

Chen Huang: Simulation, Validation, Writing – original draft, Writing – review & editing, Visualization, Project administration, Funding acquisition. Marius Bloching: Writing – original draft of experiments, explaining experimental data. Andrei Lipatnikov: Conceputualization, Methodology, Validation, Writing – original draft, Writing – review & editing, Funding acquisition.

Declaration of competing interest

The authors declare that they have no known competing financial interests or personal relationships that could have appeared to influence the work reported in this paper.

References

Bauwens, C.R., Bergthorson, J.M., Dorofeev, S.B., 2015. Experimental study of spherical-flame acceleration mechanisms in large-scale propane–air flames. Proc. Combust. Inst. 35, 2059–2066. https://doi.org/10.1016/j.proci.2014.06.118.

Bauwens, C.R., Chaffee, J., Dorofeev, S., 2008. Experimental and numerical study of methane-air deflagrations in a vented enclosure. Fire Saf. Sci. 9, 1043–1054. https://doi.org/10.3801/IAFSS.FSS.9-1043.

Bauwens, C.R., Chaffee, J., Dorofeev, S.B., 2011. Vented explosion overpressures from combustion of hydrogen and hydrocarbon mixtures. Int. J. Hydrogen Energy 36, 2329–2336. https://doi.org/10.1016/j.ijhydene.2010.04.005.

Bradley, D., 1999. Instabilities and flame speeds in large-scale premixed gaseous explosions. Philos. Trans. R. Soc. A 357, 3567–3581. https://doi.org/10.1098/rsta.1999.0510.

Bradley, D., Chen, Z., Swithenbank, J., 1989. Burning rates in turbulent fine dust-air explosions. Proc. Combust. Inst. 22, 1767–1775. https://doi.org/10.1016/S0082-0784(89)80190-0.

Bradley, D., Cresswell, T., Puttock, J., 2001. Flame acceleration due to flame-induced instabilities in large-scale explosions. Combust. Flame 124, 551–559. https://doi.org/10.1016/S0010-2180(00)00208-X.

Bray, K.N.C., Moss, J.B., 1977. A unified statistical model of the premixed turbulent flame. Acta Astronaut. 4, 291–319. https://doi.org/10.1016/0094-5765(77)90053-4.

Chomiak, J., Nisbet, J.R., 1995. Modeling variable density effects in turbulent flames—some basic considerations. Combust. Flame 102, 371–386. https://doi.org/10.1016/0010-2180(95)00001-M.

Dahoe, A.E., de Goey, L.P.H., 2003. On the determination of the laminar burning velocity from closed vessel gas explosions. J. Loss Prev. Process. Ind. 16, 457–478. https://doi.org/10.1016/S0950-4230(03)00073-1.

Dahoe, A.E., Hanjalic, K., Scarlett, B., 2002. Determination of the laminar burning velocity and the Markstein length of powder–air flames. Powder Technol. 122, 222–238. https://doi.org/10.1016/S0032-5910(01)00419-3.

Daly, B.J., Harlow, F.H., 1970. Transport equations in turbulence. Phys. Fluids 13, 2634–2649. https://doi.org/10.1063/1.1692845.

Eckhoff, R.K., 2003. Dust Explosions in the Process Industries: Identification, Assessment and Control of Dust Hazards. Elsevier.

Eckhoff, R.K., 2020. Fighting dust explosion hazards in the process industries. J. Loss Prev. Process. Ind. 67, 104225. https://doi.org/10.1016/j.jlp.2020.104225.

El Tahry, S., 1983. K-epsilon equation for compressible reciprocating engine flows. J. Energy 7, 345–353.

EN14491, 2012. Dust Explosion Venting Protective Systems. European Committee for Standardization, Brussels.

EN 14994, 2007. Gas Explosion Venting Protective Systems. European Committee for Standardization, Brussels.

Gostintsev, Y.A., Istratov, A., Shulenin, Y.V., 1988. Self-similar propagation of a free turbulent flame in mixed gas mixtures. Combust. Explos. Shock Waves 24, 563–569. https://doi.org/10.1007/BF00755496.

Gostintsev, Y.A., Istratov, A.G., Kidin, N.I., Fortov, V.E., 1999. Self-turbulization of gas flames: an analysis of experimental results. High Temp. 37, 282–288.

Gülder, Ö.L., 1984. Correlations of laminar combustion data for alternative SI engine fuels. SAE Technical Paper 841000.

Hellsten, A., 1998. Some improvements in Menter's k-omega SST turbulence model. In: 29th AIAA, Fluid Dynamics Conference, p. 2554.

Hinze, J.O., 1975. Turbulence, second ed.

Huang, C., Lipatnikov, A.N., Nessvi, K., 2020. Unsteady 3-D RANS simulations of dust explosion in a fan stirred explosion vessel using an open source code. J. Loss Prev. Process. Ind. 67, 104237. https://doi.org/10.1016/j.jlp.2020.104237.

Huang, C., Yasari, E., Johansen, L., Hemdal, S., Lipatnikov, A., 2016. Application of flame speed closure model to RANS simulations of stratified turbulent combustion in a gasoline direct-injection spark-ignition engine. Combust. Sci. Technol. 188, 98–131. https://doi.org/10.1080/00102202.2015.1083988.

Launder, B.E., Sharma, B.I., 1974. Application of the energy-dissipation model of turbulence to the calculation of flow near a spinning disc. Lett. Heat Mass Tran. 1, 131–137.

Launder, B.E., Spalding, D.B., 1972. Lectures in Mathematical Models of Turbulence.

Launder, B.E., Spalding, D.B., 1983. The numerical computation of turbulent flows. In: Numerical Prediction of Flow, Heat Transfer, Turbulence and Combustion. Elsevier, pp. 96–116.

Li, H., Chen, X., Deng, J., Shu, C.-M., Kuo, C.-H., Yu, Y., Hu, X., 2020. CFD analysis and experimental study on the effect of oxygen level, particle size, and dust concentration on the flame evolution characteristics and explosion severity of cornstarch dust cloud deflagration in a spherical chamber. Powder Technol. 372, 585–599. https://doi.org/10.1016/j.powtec.2020.05.117.

Libby, P.A., Bray, K., 1977. Variable density effects in premixed turbulent flames. AIAA J. 15, 1186–1193.

Lipatnikov, A., 2012. Fundamentals of Premixed Turbulent Combustion. CRC Press.

Lipatnikov, A.N., 2018. RANS simulations of premixed turbulent flames. In: Modeling and Simulation of Turbulent Combustion. Springer, pp. 181–240.

Lipatnikov, A.N., Chomiak, J., 1997. A simple model of unsteady yurbulent flame propagation. SAE Trans., Sect. 3, J. Engines 106, 2441–2452 (SAE Paper 972993).

Lipatnikov, A.N., Chomiak, J., 2002. Turbulent flame speed and thickness: phenomenology, evaluation, and application in multi-dimensional simulations. Prog. Energy Combust. Sci. 28, 1–74. https://doi.org/10.1016/S0360-1285(01)00007-7.

Lipatnikov, A.N., Chomiak, J., 2004. Application of the Markstein number concept to curved turbulent flames. Combust. Sci. Technol. 176, 331–358.

Lipatnikov, A.N., Chomiak, J., 2007. Global stretch effects in premixed turbulent combustion. Proc. Combust. Inst. 31, 1361–1368.

Lipatnikov, A.N., Chomiak, J., 2010. Effects of premixed flames on turbulence and turbulent scalar transport. Prog. Energy Combust. Sci. 36, 1–102. https://doi.org/10.1016/j.pecs.2009.07.001.

Magnussen, B.F., Hjertager, B.H., 1977. On mathematical modeling of turbulent combustion with special emphasis on soot formation and combustion. Proc. Combust. Inst. 16, 719–729. https://doi.org/10.1016/S0082-0784(77)80366-4.

Menter, F., Esch, T., 2001. Elements of industrial heat transfer predictions. In: 16th Brazilian Congress of Mechanical Engineering. COBEM), p. 650.

Menter, F.R., Kuntz, M., Langtry, R., 2003. Ten years of industrial experience with the SST turbulence model. Turbulence, Heat Mass Trans. 4, 625–632.

NFPA68, 2018. NFPA 68 Standard on Explosion Protection by Deflagration Venting.

Phylaktou, H., Gardner, C., Andrews, G., 2010. Flame speed measurements in dust explosions. In: Proceedings of the Sixth International Seminar on Fire and Explosion Hazards, p. e16.

Pico, P., Ratkovich, N., Muñoz, F., Dufaud, O., 2020. Analysis of the explosion behaviour of wheat starch/pyrolysis gases hybrid mixtures through experimentation and CFD-DPM simulations. Powder Technol. 374, 330–347. https://doi.org/10.1016/j.powtec.2020.07.016.

Proust, C., 1993. Experimental determination of the maximum flame temperatures and of the laminar burning velocities for some combustible dust-air mixtures. In: 5. International Colloquium on Dust Explosions, pp. 161–184.

Sabelnikov, V.A., Lipatnikov, A.N., 2017. Recent advances in understanding of thermal expansion effects in premixed turbulent flames. Annu. Rev. Fluid Mech. 49, 91–117. https://doi.org/10.1146/annurev-fluid-010816-060104.

Shih, T.-H., Liou, W.W., Shabbir, A., Yang, Z., Zhu, J., 1994. A new k-epsilon eddy viscosity model for high Reynolds number turbulent flows: model development and validation. NASA Sti/recon Tech. Rep. N 95, 11442.

Shih, T., Liou, W., Shabbir, A., Zhu, J., 1995. A new k-epsilon eddy-viscosity model for high Reynolds number turbulent flows-model development and validation. Comput. Fluid 24 (3), 227–238.

Skjold, T., 2007. Review of the DESC project. J. Loss Prev. Process. Ind. 20, 291–302. https://doi.org/10.1016/j.jlp.2007.04.017.

Skjold, T., 2014a. Simulating vented maize starch explosions in a 236 m3 silo. Fire Saf. Sci. 11, 1469–1480. https://doi.org/10.3801/IAFSS.FSS.11-1469.

Skjold, T., 2014b. Flame Propagation in Dust Clouds. Numerical Simulation and Experimental Investigation, PhD Thesis. University of Bergen.

Skjold, T., Arntzen, B.J., Hansen, O.R., Storvik, I.E., Eckhoff, R.K., 2006. Simulation of dust explosions in complex geometries with experimental input from standardized tests. J. Loss Prev. Process. Ind. 19, 210–217. https://doi.org/10.1016/j.jlp.2005.06.005.

Skjold, T., Arntzen, B.J., Hansen, O.R., Taraldset, O.J., Storvik, I.E., Eckhoff, R.K., 2005. Simulating dust explosions with the first version of DESC. Process Saf. Environ. Protect. 83, 151–160. https://doi.org/10.1205/psep.04237.

Spalding, D.B., 1971. Mixing and chemical reaction in steady confined turbulent flames. Symp. Combust. Proc. 13, 649–657. https://doi.org/10.1016/S0082-0784(71)80067-X.

Speziale, C.G., Sarkar, S., Gatski, T.B., 1991. Modelling the pressure–strain correlation of turbulence: an invariant dynamical systems approach. J. Fluid Mech. 227, 245–272. https://doi.org/10.1017/S0022112091000101.

Tan, I., Wee, C.C., Sopade, P.A., Halley, P.J., 2004. Estimating the specific heat capacity of starch-water-glycerol systems as a function of temperature and compositions. Starch Staerke 56, 6–12. https://doi.org/10.1002/star.200300209.

Taylor, G.I., 1921. Diffusion by continuous movements. Proc. London Math. Soc., Ser. 2 (20), 196–211.

Taylor, G.I., 1935. Statistical theory of turbulence. IV. Diffusion in a turbulent air stream. Proc. Roy. Soc. Lond. A151, 421–478.

Tolias, I.C., Stewart, J.R., Newton, A., Keenan, J., Makarov, D., Hoyes, J.R., Molkov, V., Venetsanos, A.G., 2018. Numerical simulations of vented hydrogen deflagration in a medium-scale enclosure. J. Loss Prev. Process. Ind. 52, 125–139. https://doi.org/10.1016/j.jlp.2017.10.014.

Van Wingerden, K., Stavseng, L., Bergen, N., 1996. Measurements of the laminar burning velocities in dust-air mixtures. VDI-Ber. 1272, 553–564.

VDI3673, 2002. Guideline VDI 3673 Part 1: Pressure Release of Dust Explosions. VDI.

Wilcox, D.C., 1998. Turbulence Modeling for CFD. DCW industries La Canada, CA.

Yakhot, V., Orszag, S., Thangam, S., Gatski, T., Speziale, C., 1992. Development of turbulence models for shear flows by a double expansion technique. Phys. Fluid. Fluid Dynam. 4, 1510–1520. https://doi.org/10.1063/1.858424.

Zimont, V.L., 1979. Theory of turbulent combustion of a homogeneous fuel mixture at high Reynolds number. Combust. Explos. Shock Waves 15, 305–311.

Zimont, V.L., 2000. Gas premixed combustion at high turbulence. Turbulent flame closure combustion model. Exp. Therm. Fluid Sci. 21, 179–186. https://doi.org/10.1016/S0894-1777(99)00069-2.